

Bose–Einstein condensates in microgravity

A. VOGEL^{1,✉}

M. SCHMIDT¹

K. SENGSTOCK¹

K. BONGS¹

W. LEWOCZKO²

T. SCHULDT²

A. PETERS²

T. VAN ZOEST³

W. ERTMER³

E. RASEL³

T. STEINMETZ⁴

J. REICHEL⁴

T. KÖNEMANN⁵

W. BRINKMANN⁵

E. GÖKLÜ⁵

C. LÄMMERZAHN⁵

H.J. DITTUS⁵

G. NANDI⁶

W.P. SCHLEICH⁶

R. WALSER⁶

¹ Institut für Laser-Physik, Universität Hamburg, Luruper Chaussee 149, 22761 Hamburg, Germany

² Institut für Physik, Humboldt-Universität zu Berlin, Hausvogteiplatz 5–7, 10117 Berlin, Germany

³ Institut für Quantenoptik, Universität Hannover, Welfengarten 1, 30167 Hannover, Germany

⁴ Laboratoire Kastler Brossel de l'E.N.S., 24 rue Lhomond, 75231 Paris Cedex 05, France

⁵ ZARM Universität Bremen, Am Fallturm, 28359 Bremen, Germany

⁶ Abteilung Quantenphysik, Universität Ulm, Albert-Einstein-Allee 11, 89069 Ulm, Germany*

Received: 30 January 2006/Revised version: 24 May 2006

Published online: 20 July 2006 • © Springer-Verlag 2006

ABSTRACT We report the current status of our cooperative effort to realize a ^{87}Rb Bose–Einstein condensate in microgravity. Targeting the long-term goal of studying cold quantum gases on a space platform, we currently focus on the implementation of an experiment at the ZARM drop tower in Bremen. Fulfilling the technical requirements for operation in this facility, the complete experimental setup will fit in a volume of less than 1 m^3 with a total mass below 150 kg and a total power consumption of the order of 625 W. The individual parts of the setup, in particular the ultra-compact laser system as a critical component, are presented. In addition, we discuss a first demonstration of the mechanical and frequency control stability of the laser modules. On the theoretical side, we outline the non-relativistic description of a freely falling many-particle system in the rotating frame of the Earth. In particular, we show that the time evolution of a harmonically trapped, collisionally interacting degenerate gas of bosons or fermions is as simple in an accelerated, rotating frame of reference as in an inertial frame. By adopting a co-moving generalized Galilean frame, we can eliminate inertial forces and torques. This leads to important simplifications for numerical simulation of the experiment.

PACS 03.75.-b; 03.75.Kk; 32.80.Pj

1 Introduction

One of the main sources of progress in physics lies in the curiosity to overcome and extend the current frontiers in parameter space and knowledge. A particularly rewarding path has been towards the achievement of ever lower temperatures, which was marked with important discoveries like

superfluidity and superconductivity at the beginning of the 20th century and temporarily culminated in the observation of Bose–Einstein condensation in 1995 [2, 6–8]. The extremely low energy scales in the nano-kelvin cold Bose–Einstein condensed atomic gases open a new experimental window for the direct study of quantum effects. The macroscopically occupied condensate wavefunction typically reaches extensions of the order of $100\ \mu\text{m}$ and can be directly imaged on a CCD camera by illumination with a laser flash. Bose–Einstein condensates (BECs) have led to fundamental insights into matter-wave interference, superfluidity and vortex lattices, solitons and four-wave mixing in matter waves, matter-wave amplification and atom lasers, quantum phase transitions such as the superfluid to Mott-insulator transition, quantum gas magnetism and controlled cold molecule production, to name only a few (for a recent review, see e.g. [3]).

Our goal is to continue the path towards lower energy scales by lifting Earth-bound laboratory restrictions and investigate Bose–Einstein condensates in a microgravity environment. There are several reasons why weightlessness is important for fundamental research on cold quantum gases.

First of all, in a microgravity environment it is possible to substantially lower the trapping potential adiabatically without the need of (noisy) levitational fields to compensate for gravity. Therefore, it is possible to reach much lower temperatures than achievable in any Earth-bound experiment. The present low-temperature record of just below 500 pK [16] corresponds to the gravitational potential energy of a Rb atom at a height of 5 nm, which is much smaller than the typical extension of a condensate. Therefore, gravity is a major perturbation to the system in the low-temperature regime.

In the resulting ultra-large condensates, possibly extending over 10 mm, it is possible to gain absolute control of the macroscopic matter wave, as optical readout and manipulation can be performed with very high relative spa-

✉ Fax: +494089985295, E-mail: avogel@physnet.uni-hamburg.de

*for the QUANTUS collaboration

tial resolution. Furthermore, the effect of ultra-weak long-range forces becomes important in these condensates, which promises the discovery of new kinds of low-energy phase transitions. Another important point is that the time of free and unperturbed evolution can be significantly longer than in earthbound laboratories. This is crucial for atom interferometric metrology such as with atomic clocks, which are pursued in the PHARAO and ACES collaborations (see e.g. [5]). The precision of these and also gravitational sensors might be extended by up to three orders of magnitude in microgravity.

We finally want to emphasize that weightlessness is a major advantage for research on mixtures of quantum gases, as atoms with different masses do not experience different potentials and can be perfectly overlapped in the trap. Experiments on cold quantum gases under microgravity therefore promise to give insights into new low-temperature phenomena and the effect of long-range forces in regimes never accessible before. It will boost actual developments in the field of degenerate quantum gases, in particular with respect to fundamental physics, such as basic quantum correlations, fundamental measurement limitations, decoherence, entanglement, and quantum phases (e.g. superfluidity, Mott insulators).

In this paper, we present the status of our cooperative effort to realize Bose–Einstein condensation in a microgravity environment, with the long-term goal of establishing an experimental platform in space to allow investigations in free fall for unlimited time. Besides the various space options (e.g. international space station, its automated transfer vehicles for supply delivery, and dedicated satellites) there are several short-term options of how to place an experimental setup in weightlessness. As a first step we aim at establishing a device that generates a degenerate quantum gas in the drop tower at ZARM¹ in Bremen, Germany. Such an experiment will differ from common Earth-bound setups to a large extent and we have to address new technical challenges, which in several respects are similar to the requirements of a space platform. The boundary conditions and the corresponding experimental layout will be discussed in addition to the presentation of first stability measurements of the laser system. Moreover, we will give an introduction to the theoretical description of a freely falling degenerate quantum gas and define a suitable co-moving frame of reference, in which analytical and numerical calculations become more efficient than in the Earth-fixed frame.

The drop capsule holding the setup (Fig. 1) reaches excellent acceleration suppression down to the microgravity level of 10^{-6} g, while it falls freely in the evacuated drop-tower tube for about 5 s. In the catapult operation mode this duration can be extended even up to 9 s. The repetition rate of three drops per day is limited by the time needed to evacuate the tube and to retrieve the capsule from the deceleration unit. For technical optimization tasks, such as adiabatic expansion studies, the same setup can be placed in a zero-g ($\approx 10^{-2}$ g) aircraft that can perform up to 30 consecutive parabolic flights, each lasting about 20 s. However, the drop tower is preferable for the targeted final experiments as the residual acceleration is smaller by four orders of magnitude. Moreover, it is more easily accessible in the development phase. In Sect. 2, we will

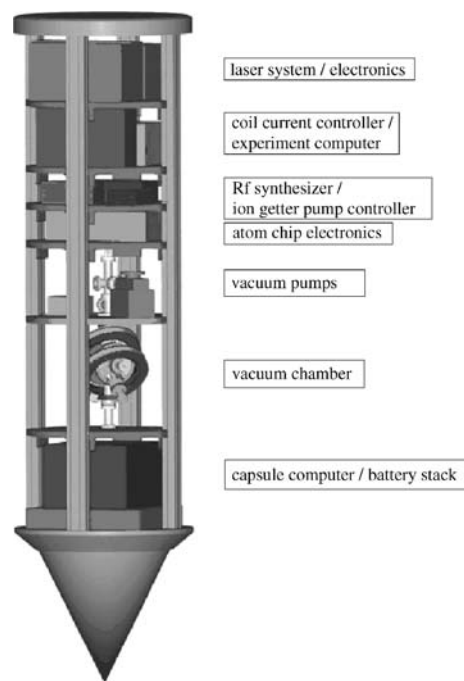


FIGURE 1 The interior of the drop capsule (a μ -metal magnetic shield and the aluminum enclosure of the capsule are omitted for clarity)

discuss the technical requirements of such a cold atom experiment at a drop tower.

2 Experimental setup

The experimental techniques for the realization of Bose–Einstein condensation in dilute atomic gases are extensively discussed in the literature (see e.g. [13]). In short, the main requirements are a near-perfect thermal decoupling from the environment using contact-free storage in ultra-high-vacuum conditions (typically below 10^{-10} mbar) and a sophisticated two-stage trapping and cooling process. In the first stage the atoms are trapped and precooled using laser cooling in a magneto-optical trap (MOT). After reaching the corresponding temperature limit in the μ K range the sample is transferred to a conservative trapping potential (in our case realized by a magnetic field minimum) and further cooled by evaporative cooling (i.e. removing the hottest atoms from the trap, while the remaining ones rethermalize). In order to keep the setup as simple as possible, we chose ^{87}Rb for the experiment, as it has a simple laser cooling scheme for which small-size and robust diode lasers are available. It can be released into the vacuum chamber using commercially available current-controlled dispensers². Furthermore, the high ratio between elastic and inelastic scattering rates in ^{87}Rb – ^{87}Rb collisions is advantageous for evaporative cooling, and a long condensate lifetime can be achieved.

For operation in a drop tower, our experimental setup has to fulfill certain requirements that in many aspects are very similar to the ones required for operation in a satellite or an orbital space station.

Miniaturization A laboratory-based cold quantum gas experiment usually has the size of one or two optical tables

¹ www.zarm.uni-bremen.de

² SAES getters.

plus the same amount of electronic racks. We have to fit our setup into the drop capsule shown in Fig. 1 ($60 \times 60 \times 215$ cm); hence, miniaturization is a crucial point for the vacuum chamber as well as the laser system and electronics.

Low weight The drop capsule can carry a maximum weight of 230 kg. In future space missions weight is an important factor in terms of cost.

Low total power consumption The experiment is powered by a battery stack in the bottom of the drop capsule that has limited energy. Of course, power consumption has to be reduced to a minimum in space applications.

High mechanical stability Our experiment has to withstand the deceleration of approximately 50 g at the end of the drop. Yet it is even more important to maintain the stability of the laser frequency and intensity at the moment of release. In future space missions the experiment must not be permanently misaligned from shocks and vibrations experienced during the launch phase.

Low cycle times At the moment of release, the trapped gas will be in the MOT phase in order to damp out probable vibrations of the drop capsule after release in the non-conservative light force. Therefore all following cooling phases, in particular the evaporation, have to be faster than the time of 4.74 s available in weightlessness to investigate the condensate.

Automation While the drop tower is evacuated for two hours, the experiment is only accessible via remote control. During the drop the experiment is under computer control. All data is recorded by the computer system, which is installed in the drop capsule.

In order to meet the need of short evaporation times and low power consumption, we use a magnetic microtrap on a chip reaching strong magnetic confining potentials with moderate currents. The vacuum chamber is made from steel with a very low magnetic permeability resulting in high mechanical stability and low field disturbances. In Sects. 2.1 and 2.2 we will briefly describe the atom chip and the vacuum chamber and how they meet the requirements. Then, we concentrate on the laser system as its stability is critical for the success of this experiment.

2.1 Magnetic chip trap

We choose a magnetic trap on a chip [12, 19, 21] to fit our needs regarding low size and power consumption. Most importantly the chip contains a *U*-shaped wire producing a quadrupole field for the operation of an on-chip MOT and a *Z*-shaped wire for the creation of an Ioffe-type magnetic trap (Fig. 2). The additional straight wire creates a strongly confining ‘dimple’ in the weak axis of the Ioffe trap and also significantly reduces the trap aspect ratio, an advantage for later adiabatic expansion. The dimple trap provides trap frequencies in the (*x*, *y*, *z*) directions of about (1, 3, 3) kHz at currents of 2 A and 1 A through the *Z*-shaped and the straight wires, respectively, allowing evaporation times of the order of one second, well within the time of free fall.

Both the *U*- and the *Z*-chip traps need an external bias field that has to be provided by coils around the vacuum chamber.

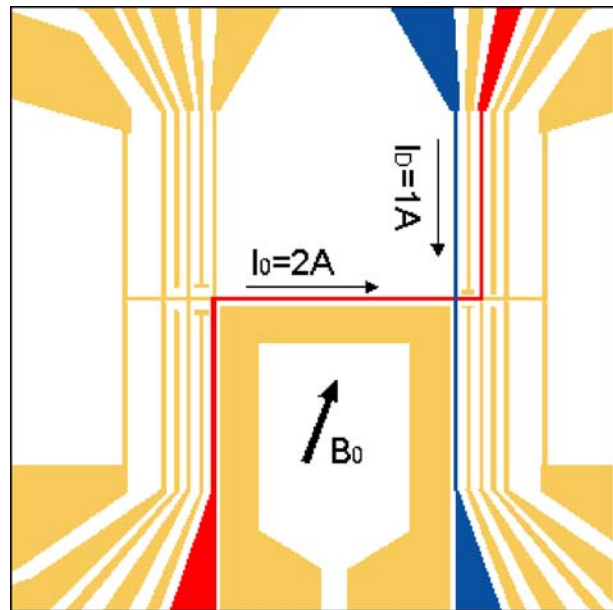


FIGURE 2 Layout of the trapping chip

A dielectric layer glued on top of the chip acts as a mirror for the cooling lasers to realize a four-beam mirror MOT.

The atom-chip technique has several advantages over a conventional BEC experiment: in order to realize all the magnetic field configurations that are required to prepare a BEC with conventional external coils an electrical power in the range of 1 kW is needed. An atom chip requires only a power of the order of 10 W. However, the coils for the external bias field and the external MOT quadrupole field consume a power of approximately 350 W. Furthermore, the confinement in the magnetic trap generated by an atom chip is stronger by one order of magnitude compared with magnetic traps realized with external coils, which leads to shorter evaporation times due to faster rethermalization. The advantages of the chip setup, relying on a tight confinement close to the surface, will be used to create BECs in a quick and efficient way. After this preparation phase the trapping potential will be significantly reduced and moved several mm away from the surface to avoid surface interaction effects.

2.2 Vacuum chamber

The atom chip is mounted in a non-magnetic stainless steel vacuum chamber. The chamber is kept at low pressure (10^{-10} mbar) by a titanium sublimation pump and an ion-getter pump. Additionally, the evaporated rubidium acts as a getter. As mentioned above, the atom chip needs a magnetic bias field, which is created by a pair of coils in Helmholtz configuration outside the vacuum chamber (65 G at 6.5 A). The external MOT needs a magnetic field gradient, which is provided by two coils in anti-Helmholtz configuration (10 G/cm at 7 A). These two pairs of magnetic coils are water cooled. Two pairs of smaller coils complete the possibility of correcting for offsets in the *x*, *y*, and *z* plane. Thus, external fields (e.g. the Earth’s magnetic field) can be compensated and precise positioning of the atomic cloud can be realized. The laser light needed to prepare and detect the atomic en-

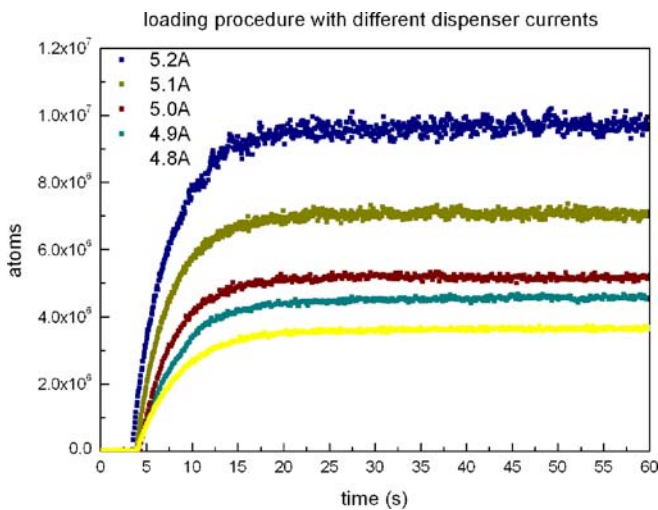


FIGURE 3 Loading rate of the MOT with various dispenser currents

semble is transmitted to the vacuum chamber via polarization-maintaining optical fibers and is expanded to a size of 20 mm with a telescope arrangement. All optics are rigidly attached to the steel body of the vacuum chamber, giving maximum stability and minimizing possible sources of misalignment.

For redundancy and operation lifetime there are three ^{87}Rb dispensers mounted in the vacuum chamber. In order to keep the complexity as low as possible, the MOT is directly loaded from a rubidium background gas, the pressure of which has to be optimized as a trade-off between loading rate and lifetime of the MOT. In addition to the relatively slow pressure adjustment via the dispenser current, we are currently optimizing our control on the ^{87}Rb adsorption layer on the chamber walls. In order to temporarily desorb rubidium atoms from the chamber walls and therefore switch between a high rubidium partial pressure for rapidly loading the MOT and a low background pressure to achieve longer MOT lifetimes, light induced atom desorption (LIAD) is used [1], using eight UV LEDs (Roithner Lasertechnik) with 16 mW of power each. So far, using only LIAD with the rubidium dispensers switched off, atom numbers of the order of 5×10^5 have been achieved. With running dispensers, atom numbers of approximately 1×10^7 have been achieved, with a loading time which still indicates an adequate pressure (about 5 s, see Fig. 3)³.

2.3 Laser system

As previously noted, the laser system has to provide stable frequencies and intensities during the drop. To prepare and analyze a Bose–Einstein condensate of ^{87}Rb , we need four frequencies with a bandwidth not much greater than 1 MHz in two different frequency classes at a wavelength of about 780.24 nm. The relevant electronic energy levels of ^{87}Rb with the needed frequencies are shown in Fig. 6. A power of about 50 mW at the atom cloud will be needed on the cooling transition, while a few mW of power are sufficient for the other frequencies.

³ These early measurements were performed with laboratory laser systems. In similar experiments with the miniature laser systems, even better performance was observed due to the higher available power.

2.3.1 DFB laser diode. For reasons of mechanical stability we use distributed feedback (DFB) laser diodes, which have an intrinsic grating in the active semiconductor area to obtain narrow bandwidths, rather than the commonly used setup with an external resonator (grating or etalon). DFB diodes from Eagleyard (EYP-DFB-0780-00080-1500-TOC03-0000) mounted in a TO3 housing with an internal Peltier cooler perfectly fit our requirements regarding size. This kind of diode laser provides a power of 80 mW at an operational current of 140 mA and can be directly used to supply light for the repumping transition. In order to deliver enough cooling light to the atoms in the vacuum chamber, the light has to be amplified to compensate for losses at the optical components and fiber coupling. Our DFB lasers can be tuned in wavelength by changing either temperature or current with the coefficients $d\lambda/dT = (0.0540 \pm 0.0007)$ nm/K and $d\lambda/dI = (2.7 \pm 0.2)$ nm/ μA , respectively. Due to the high tuning coefficient in the operational current, we have to demand that the current driver has an extremely low signal to noise ratio, in order not to broaden the emitting bandwidth. Hence, we do not use a commercial design but have implemented a current driver based on the design described in [17].

To assure that the bandwidth is of the order of a few MHz, we measured the beat note of two independent, freely running lasers. A typical measurement curve is shown in Fig. 4, which illustrates that it is possible to resolve the Doppler-free spectrum of rubidium. DFB lasers have an extremely wide range of mode-hop-free operation, so it is possible to measure the spectrum of the whole D2 lines of ^{87}Rb and ^{85}Rb in a single scan, which is shown in Fig. 5. In addition, this is an advantage for future automated locking techniques. Rubidium spectroscopy with DFB lasers is described in [15].

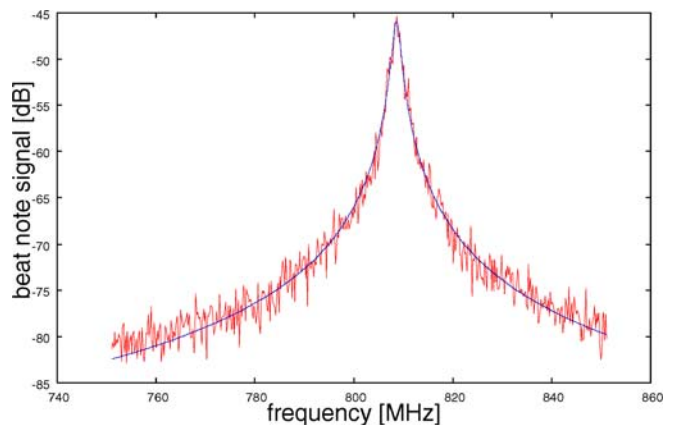


FIGURE 4 Typical width of a beat note between two freely running DFB lasers

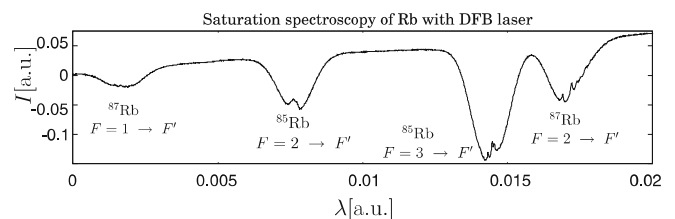


FIGURE 5 A mode-hop-free scan of the D2 lines of ^{87}Rb and ^{85}Rb in saturation spectroscopy

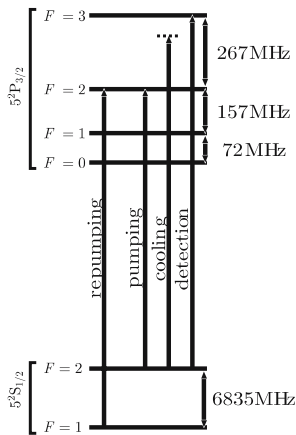


FIGURE 6 Energy-level diagram of the D2 transition of ^{87}Rb showing the frequencies needed for preparation and detection of a BEC

2.3.2 General concept. Figure 6 shows that the repumping transition is separated from the cooling, detection, and pumping frequencies by about 6.8 GHz. The latter frequencies are separated by no more than 270 MHz and can be derived from a single laser by using acousto-optic modulators (AOMs). However, a second laser is needed for the repumping transition and the minimal concept has to include two laser diodes.

We investigate two options for the implementation of the laser system. As noted above, we need an amplifier to achieve large enough laser powers at the vacuum chamber for cooling the condensate. The minimal system required is therefore a stabilized master laser and a second amplified laser (master oscillator power amplifier, MOPA) that is offset locked to the master. In this case, the master has to be locked to one of the transitions in the D2 $F = 1 \rightarrow F'$ manifold, all of which are relatively weak, in order to be able to shift its frequency to the repumping transition by means of an AOM. The second concept which promises a higher lock stability is to lock a master laser to the strongest transition of ^{87}Rb or even ^{85}Rb and offset lock both a single and an amplified laser to the master laser. In this concept, however, three lasers are needed, which is a disadvantage in size, weight, and power consumption.

For optimization of the laser lock, two methods for resolving the hyperfine structure are evaluated: the Doppler-free dichroic atomic vapor laser lock (DFDL) [20, 24] and modulation transfer spectroscopy [23]. The DFDL is a relatively new technique with a very compact setup; the other is a well-established and reliable technique with more components and electronics. A scheme/photograph of the setup for the DFDL master is shown in Figs. 7 and 8.

2.3.3 MOPA. In order to amplify the laser light in the MOPA system, we chose a tapered amplifier from Eagleyard (EYP-TPA-0780-00500-3006-CMT03-0000). It produces up to 500 mW of laser power at an operational current of 1.5 A and an incoming saturation power of 50 mW. The emerging beam is circularized using a setup with a cylindrical lens as described in [25]. With our setup (Fig. 8), we achieve fiber coupling efficiencies of 45%. We use single-mode, polarization-maintaining fibers with an 8° -angled polish to prevent back reflections forming resonators inside the laser setup.

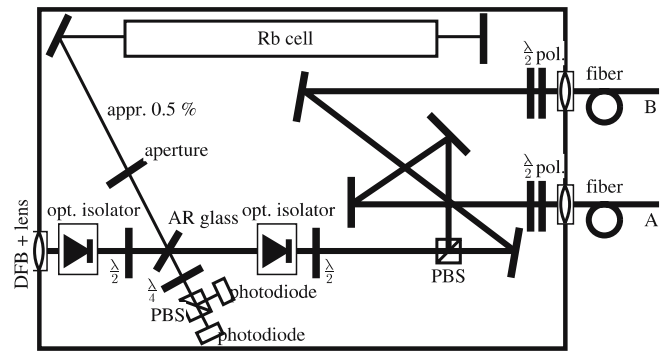


FIGURE 7 Schematic setup of the DFDL master laser

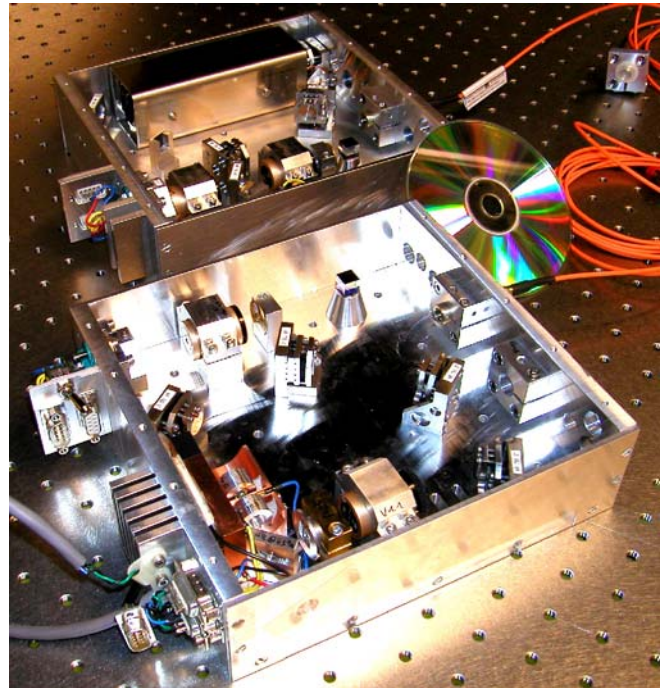


FIGURE 8 MOPA system (front) and master laser system (back) in comparison to a compact disc

2.3.4 Mounting the laser modules. To be flexible, we placed all functional units, e.g. master laser, MOPA, light intensity control by AOM, in separate modules that are held by a 19" housing, compatible with standard electronic rack widths. All mounts for optical components were specially designed by us with a beam height of 20 mm for maximum stability. The 19" housing that holds the modules and the modules themselves were made of stress-free aluminum. Adjustable mirror mounts were made from stainless steel for higher stability, as the mirror mounts are the crucial part for fiber coupling stability. The laser system including the control electronics has a total mass of about 45 kg.

2.3.5 Stability tests. In order to test the system stability, measurements in the drop tower with only the laser system were carried out. Figure 9 shows the stability of the fiber coupling. There is only a small jitter of less than 1% in laser output power from the fiber at the release of the drop capsule ($1g \rightarrow 0g$ transition).

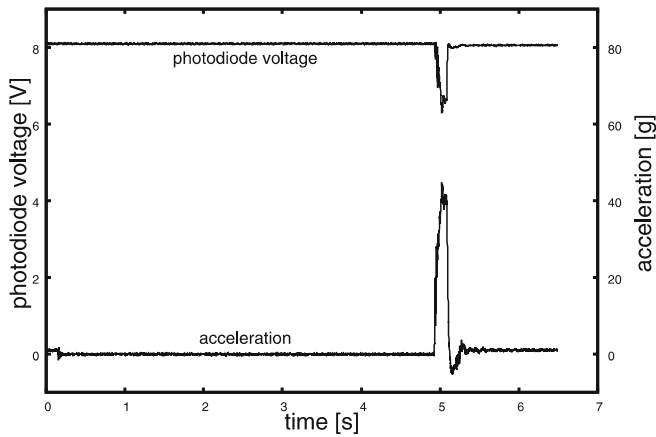


FIGURE 9 Stability of fiber coupling during a drop experiment. The measured photodiode voltage is proportional to the laser power transmitted by the fiber. The lower curve shows the acceleration of the drop capsule

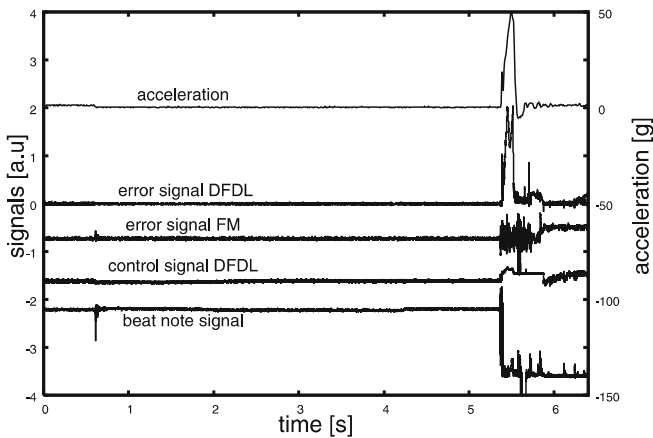


FIGURE 10 Frequency stability of both DFDL (Doppler-free dechroic atomic vapor-laser lock) and FM (frequency modulation) lock master lasers during a drop experiment. Acceleration of the drop capsule, error signals of both DFDL and FM lock master lasers, and the control signal of the DFDL master laser are plotted together with a signal that is proportional to the peak frequency of the beat note of both lasers

At the moment of impact at the bottom of the drop tower, the deceleration reached ≈ 40 g and the laser power transmitted by the fiber dropped temporarily to 78% of its initial value. The frequency-lock stability during a flight is plotted in Fig. 10. In this experiment we recorded a beat note between both our laser-lock concepts, where both lasers were locked to the same transition ($^{87}\text{Rb } F = 2 \rightarrow \text{crossover } F' = 2, 3$). Both lasers remained locked at the moment of release and during the flight; however, at the moment of impact both lasers lost frequency stability.

The test results indicate that the laser system meets all the conditions for drop experiments. They also suggest that slight improvements might be sufficient to meet the challenges of experiments at the drop tower in catapult operation, which is work currently in progress.

3 Theoretical description

In this section we want to focus on the theoretical description of a freely falling many-particle system, in particular a BEC. In common laboratory experiments free expan-

sion times are usually limited to a few ms. Thus, the spreading of the wavefunction is comparable in size with the distances covered by the motion of the center of mass. Consequently, one can employ the same spatial grid discretization in numerical simulations to describe the condensate before as well as during the free fall. However, in the drop-tower experiment, the center of mass of the atomic cloud moves more than 100 m and therefore it is crucial to transform to a co-moving frame of reference.

The drop tower is located in Bremen at the geographical latitude of $53^\circ 04' 37''$ N and a longitude of $8^\circ 48' 35''$ E. Hence, it is also necessary to consider the rotation of the Earth. In the following sections, we will revisit the classical mechanics of a single trapped particle falling in a rotating frame. Then, we will introduce the non-relativistic quantum mechanical description of a single atom. Finally, we will use the language of second quantization to incorporate the statistics as well as the binary interaction amongst particles. With these tools at hand, we will show that the evolution of the interacting, freely falling, harmonically trapped, many-particle system in a rotating frame is as simple as the evolution in an inertial frame. This generalizes the equivalence principle to harmonically trapped, interacting particles. These conclusions are found without explicit reference to the conventional mean-field Gross–Pitaevkii picture and thus provide stringent tests of more sophisticated theories.

3.1 Single-particle mechanics of the free fall in a rotating frame

3.1.1 Motion of the drop capsule. Let us first consider the classical Newtonian equation of motion of the drop capsule in a rotating frame of the Earth. The center-of-mass coordinate of the drop capsule will be denoted by \mathbf{r} and we want to assume for simplicity that it coincides with the center of the atomic trap. Furthermore, we will position the origin of the Earth-fixed coordinate system (x, y, z) at the top of the drop tower (see Fig. 11). It is of practical relevance to note that the drop tower does not point towards the center of the Earth but there is a misalignment of the plummet due to the geoidal shape of the Earth. This means that – in the model of a per-

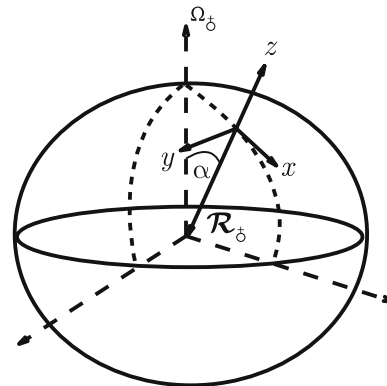


FIGURE 11 The origin of the Earth-fixed coordinate system (x, y, z) is at the top of the drop tower and co-rotating with the Earth (angular velocity Ω_{\oplus}). The position vector pointing to the center of the Earth is denoted by \mathcal{R}_{\oplus} . $\pi/2 - \alpha$ refers to the angle of the latitude at which the drop tower is situated ($53^\circ 04' 37''$ N)

fect fluid – the surface of the Earth is shaped in such a way that tangential forces, originating from the centrifugal force, must vanish [11]. Gravitational quadrupole and higher moments arising from the geoidal description will be neglected, though.

In the Earth-fixed frame, one finds the Newtonian equation of motion for the center of the drop capsule:

$$\mathcal{M}\ddot{\mathbf{r}} = \mathbf{F}_{\text{cor}} + \mathbf{F}_{\text{cent}} + \mathbf{F}_{\text{grav}}, \quad (1)$$

with the Coriolis force

$$\mathbf{F}_{\text{cor}} = -2\mathcal{M}\boldsymbol{\Omega}_{\oplus} \times \dot{\mathbf{r}}, \quad (2)$$

the centrifugal force

$$\mathbf{F}_{\text{cent}} = -\mathcal{M}\boldsymbol{\Omega}_{\oplus} \times [\boldsymbol{\Omega}_{\oplus} \times (\mathbf{r} + \mathcal{R}_{\oplus})], \quad (3)$$

and the gravitational force

$$\mathbf{F}_{\text{grav}} = -\gamma \frac{M_{\oplus}\mathcal{M}}{|\mathbf{r} + \mathcal{R}_{\oplus}|^3} (\mathbf{r} + \mathcal{R}_{\oplus}). \quad (4)$$

Here, \mathcal{M} and M_{\oplus} denote the masses of the drop capsule and the Earth, respectively. As usual, γ represents the gravitational constant, \mathcal{R}_{\oplus} is the position vector of the center of the Earth in the coordinate system fixed to the tower, and $\boldsymbol{\Omega}_{\oplus}$ is the angular velocity of the Earth; see also Fig. 11. In the derivation, we have also assumed that the change of the rotation rate of the Earth is negligible on the time scale of the experiment. Since the center-of-mass coordinate \mathbf{r} of the drop capsule is limited by the height of the drop tower, which is much smaller than the radius of the Earth \mathcal{R}_{\oplus} , we can linearize (4). Hence, we arrive at the classical equation of motion

$$\ddot{\mathbf{r}} = -2\boldsymbol{\Omega}_{\oplus} \times \dot{\mathbf{r}} - \boldsymbol{\Omega}_{\oplus} \times (\boldsymbol{\Omega}_{\oplus} \times \mathbf{r}) - \mathbf{g}, \quad (5)$$

where the gravitational acceleration vector is introduced via

$$\mathbf{g} \equiv -\gamma \frac{M_{\oplus}}{|\mathcal{R}_{\oplus}|^3} \mathcal{R}_{\oplus} - \boldsymbol{\Omega}_{\oplus} \times (\boldsymbol{\Omega}_{\oplus} \times \mathcal{R}_{\oplus}). \quad (6)$$

On the surface of the Earth, \mathbf{g} defines the z -direction being perpendicular to the ground. We followed the standard way of treating a freely falling point mass on the Earth [11]. \mathbf{g} contains a centrifugal part with components in y - and z -directions besides the leading term, which is due to gravity.

The linear equation (5) can be solved easily for the parameters of the drop tower ($h = 110$ m, $\tau = 4.74$ s, $|\boldsymbol{\Omega}_{\oplus}| = 7.27 \times 10^{-5}$ 1/s). One can also safely disregard the centrifugal term $\boldsymbol{\Omega}_{\oplus} \times (\boldsymbol{\Omega}_{\oplus} \times \mathbf{r})$, which is of the order of 10^{-7} m/s².

3.1.2 Motion of a trapped atom. Now, we want to consider a single atomic particle with mass m , which is trapped harmonically inside the drop capsule (see Fig. 12). The center of the trap coincides with the center of mass of the drop capsule \mathbf{r} and is moving on the classical trajectory given by (1). The classical Hamiltonian function then reads

$$H_0(\mathbf{r}, \mathbf{p}) = \frac{\mathbf{p}^2}{2m} - \boldsymbol{\Omega}_{\oplus} \cdot \mathbf{l} + m\mathbf{g} \cdot \mathbf{r} + [\mathbf{r} - \boldsymbol{\tau}(t)]^{\top} \frac{m\omega^2(t)}{2} [\mathbf{r} - \boldsymbol{\tau}(t)]. \quad (7)$$

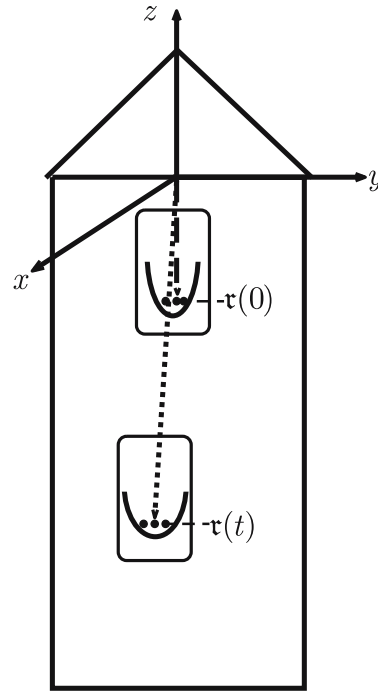


FIGURE 12 Drop tower with falling drop capsule. Inside the capsule one can see the harmonic trap constraining the motion of the atomic gas. $\boldsymbol{\tau}(0)$ is the center-of-mass coordinate of the drop capsule at the moment of release, $\boldsymbol{\tau}(t)$ corresponds to the center-of-mass coordinate at a later instant

Here, we have introduced the angular momentum of the particle as $\mathbf{l} = \mathbf{r} \times \mathbf{p}$. The three-dimensional trapping potential is not necessarily isotropic but of general shape according to the specifications of Sect. 2.1. Thus, we consider a time-dependent matrix of trap frequencies $\omega(t)$. Via Hamilton's equations of motion, one easily obtains the classical equation of motion

$$\ddot{\mathbf{r}} = -2\boldsymbol{\Omega}_{\oplus} \times \dot{\mathbf{r}} - \boldsymbol{\Omega}_{\oplus} \times (\boldsymbol{\Omega}_{\oplus} \times \mathbf{r}) - \omega(t)^2 (\mathbf{r} - \boldsymbol{\tau}(t)) - \mathbf{g}. \quad (8)$$

Please note that the motion of the trap due to the free fall of the drop capsule has to be taken into account.

In order to arrive at a quantum mechanical description of the particle, the quantities \mathbf{r} and \mathbf{p} become operators satisfying the commutation relation

$$[\mathbf{r}, \mathbf{p}] = i\hbar \mathbf{1}, \quad (9)$$

and the corresponding Hamiltonian operator H_0 in single-particle Hilbert space follows directly from its classical counterpart of (7). In order not to overload the notation, we will not distinguish explicitly operators in this first quantization from the classical canonical variables.

3.2 Description of a freely falling degenerate quantum gas in a rotating frame

We will show in this section that the time evolution of a harmonically trapped, collisionally interacting degenerate gas of bosons or fermions is as simple in an accelerated, rotating frame of reference as in an inertial frame. By using generalized Galilean transformations with time-dependent parameters $\mathcal{R}(t)$ and $\mathcal{P}(t)$, that are instantaneously

connected to the center of mass of the many-particle system, one can eliminate linear inertial forces and torques. These parameters follow non-trivial classical equations of motion that have to be determined. This holds true even in the presence of two-particle interactions and the harmonic confinement of the atoms. This statement is known as a generalized Kohn theorem [9, 14].

We will choose the picture of second quantization to describe the many-particle quantum system. Here, we want to focus on identical bosons, but would like to point out that our considerations are also valid for the fermionic case, i.e. they are independent of the statistical properties of the particles [4].

The dynamics of the bosonic system is determined by Heisenberg's equation of motion for the field operators $\hat{a}(\mathbf{r})$, i.e.

$$i\hbar \frac{d}{dt} \hat{a}(\mathbf{r}) = [\hat{a}(\mathbf{r}), \hat{H}] , \quad (10)$$

where \hat{H} is the second-quantized Hamiltonian, which will be determined explicitly below. The field operators satisfy the bosonic commutation relations

$$[\hat{a}(\mathbf{r}), \hat{a}^\dagger(\mathbf{r}')] = \delta^{(3)}(\mathbf{r} - \mathbf{r}') . \quad (11)$$

The properties of the single-particle operators representing the density, the center-of-mass coordinate, the total momentum, and the total angular momentum in the picture of the first quantization translate straight to operators in Fock space [10]. Thus, we will introduce the corresponding second-quantized operators of total particle number \hat{N} , collective position $\hat{\mathbf{R}}$, momentum $\hat{\mathbf{P}}$, and angular momentum $\hat{\mathbf{L}}$ as

$$\begin{aligned} \hat{N} &= \int d^3r \hat{a}^\dagger(\mathbf{r}) \hat{a}(\mathbf{r}), & \hat{\mathbf{L}} &= \int d^3r \hat{a}^\dagger(\mathbf{r}) \left[\mathbf{r} \times \frac{\hbar}{i} \nabla \right] \hat{a}(\mathbf{r}), \\ \hat{\mathbf{R}} &= \int d^3r \hat{a}^\dagger(\mathbf{r}) \mathbf{r} \hat{a}(\mathbf{r}), & \hat{\mathbf{P}} &= \int d^3r \hat{a}^\dagger(\mathbf{r}) \frac{\hbar}{i} \nabla \hat{a}(\mathbf{r}). \end{aligned} \quad (12)$$

The commutation relation for the collective coordinate and linear momentum reads

$$[\hat{\mathbf{R}}, \hat{\mathbf{P}}] = i\hbar \hat{N} . \quad (13)$$

All these operators conserve the particle number and hence commute with the number operator.

The second-quantized Hamiltonian reads

$$\hat{H} = \hat{H}_0 + \hat{V} . \quad (14)$$

Here,

$$\hat{H}_0 = \int d^3r d^3r' \hat{a}^\dagger(\mathbf{r}') \langle \mathbf{r}' | H_0 | \mathbf{r} \rangle \hat{a}(\mathbf{r}), \quad (15)$$

where $\langle \mathbf{r}' | H_0 | \mathbf{r} \rangle$ represents the matrix element in the position representation of the single-particle Hamiltonian H_0 analogous to the classical Hamiltonian function of (7). As we want to consider a dilute quantum gas, we have to take into account only binary collisions. The corresponding potential can be written in the form

$$\hat{V} = \frac{1}{2} \int d^3r d^3r' \hat{a}^\dagger(\mathbf{r}') \hat{a}^\dagger(\mathbf{r}) V(|\mathbf{r} - \mathbf{r}'|) \hat{a}(\mathbf{r}) \hat{a}(\mathbf{r}') . \quad (16)$$

In the energy range of a standard rubidium BEC, isotropic s -wave scattering is the dominant contribution to the two-particle interaction. It is sometimes convenient to introduce pseudopotentials like the contact interaction to model this type of scattering. However, such considerations are not necessary here as long as the binary potential $V(|\mathbf{r} - \mathbf{r}'|)$ depends only on the distance between the particles, i.e. it is translationally invariant.

3.3 Transformation to a co-moving frame

As mentioned above, Heisenberg's equation of motion (10) determines the full dynamics of the interacting quantum system. So far, we described the physics of the system in the Earth-fixed frame. Now we would like to make a unitary transformation \hat{U} to the co-moving freely falling frame, thus eliminating gravitational forces. In the same spirit, we can also eliminate inertial torques. Hence, we make an additional transformation to a non-rotating frame. In general, this cannot be done for an anharmonically trapped system, for example a square-well potential or superharmonic trap. But it is possible for strictly harmonically confined systems. In different contexts, this has been reported earlier [4, 9, 14].

To connect the two descriptions, i.e. the system falling with the drop capsule $\hat{a}_F(\mathbf{r})$ and the system described by the Earth-fixed reference frame $\hat{a}(\mathbf{r})$, we need to unitarily connect them via

$$\hat{a}_F(\mathbf{r}, t) = \hat{U}^{-1}(t) \hat{a}(\mathbf{r}, t) \hat{U}(t) . \quad (17)$$

We are now able to rewrite Heisenberg's equation of motion:

$$\begin{aligned} i\hbar \frac{d}{dt} \hat{a}_F(\mathbf{r}) &= [\hat{a}_F(\mathbf{r}), \hat{U}^{-1} \hat{H} \hat{U} + i\hbar \hat{U}^{-1} (\partial_t \hat{U})] \\ &\equiv [\hat{a}_F(\mathbf{r}), \hat{H}_F] . \end{aligned} \quad (18)$$

This defines a new Hamiltonian operator \hat{H}_F for a general, so far unspecified $\hat{U}(t)$.

In the following, we will construct an explicitly time-dependent transformation such that all frame-dependent terms of the Hamiltonian operator can be eliminated. For this purpose, we introduce a dynamical phase $\varphi(t)$, a center-of-mass coordinate $\mathcal{R}(t)$, and a center-of-mass momentum $\mathcal{P}(t)$ and parameterize the unitary transformation by them:

$$\hat{U}(t) = e^{i\varphi(t)/\hbar} \hat{U}_L(t) \hat{U}_R(t) \hat{U}_P(t) . \quad (19)$$

Initially, the drop capsule is at rest in the Earth-fixed frame. After release, its motion cannot induce any additional rotation to the system. Consequently, the transformation

$$\hat{U}_L = e^{-it\Omega_{\hat{\mathbf{L}}}/\hbar} , \quad (20)$$

which is the generator of the rotation around the $\Omega_{\hat{\mathbf{L}}}$ -axis, should be sufficient to cancel all rotation-dependent terms.

Apart from the rotations, we also have to consider the translations in the position and momentum space:

$$\hat{U}_R = e^{-i\mathcal{P}(t)\hat{\mathbf{R}}/\hbar} , \quad \hat{U}_P = e^{i\mathcal{R}(t)\hat{\mathbf{P}}/\hbar} , \quad (21)$$

which form the generalized Galilean transformations [22]. The parameters $\mathcal{R}(t)$ and $\mathcal{P}(t)$ are so far still undetermined classical quantities. By putting (19) into (18), we obtain

$$\hat{H}_F = \int d^3r \hat{a}_F^\dagger(\mathbf{r}) \left[-\frac{\nabla^2}{2m} + \mathbf{r} \frac{m\omega^2(t)}{2} \mathbf{r} \right] \hat{a}_F(\mathbf{r}) + \frac{1}{2} \int d^3r d^3r' \hat{a}_F^\dagger(\mathbf{r}) \hat{a}_F^\dagger(\mathbf{r}') V(|\mathbf{r} - \mathbf{r}'|) \hat{a}_F(\mathbf{r}) \hat{a}_F(\mathbf{r}'). \quad (22)$$

This requires that $\mathcal{R}(t)$, $\mathcal{P}(t)$ and the dynamical phase $\varphi(t)$ satisfy certain classical equations of motion, which can be solved. Thus, \hat{U} is determined explicitly. In (22) it was assumed that the trap frequencies in all spatial directions are equal or, more generally, that the symmetry axis of the trap is aligned with the rotational axis of the Earth. Details of these considerations will be presented in a forthcoming publication [18].

As a result, we find that all further calculations can be made in the freely falling frame, where Heisenberg's equation of motion is free of inertial forces and torques, provided that we solve the additional classical equations of motion. This is of great practical value for numerical simulations, as we only have to solve the system where the condensed gas is localized.

4 Summary

In summary, we have discussed an experimental setup and laid the foundations for a simplified theoretical description of Bose–Einstein condensates in weightlessness at the drop-tower facility of ZARM (Bremen, Germany). In addition to the vacuum and atom-chip setup, the laser system has been discussed in detail and its stability in frequency and intensity has been demonstrated to be sufficient for drop experiments. The next step will be to integrate the individual components and produce a BEC first in an Earth-bound and then in a microgravity environment accompanied by numerical simulations for this new experimental environment. Future experiments include the achievement of lowest temperatures and the observation of the evolution of correlations during slow long-term expansion. Current work is concentrating on enhancing the laser system stability to meet the specifications

for the catapult operation at the drop tower. To our knowledge, this will be the first BEC experiment in a drop tower worldwide and will open new perspectives of investigations on cold quantum gases.

ACKNOWLEDGEMENTS We gratefully acknowledge support from the Deutsche Luft- und Raumfahrtgesellschaft in the Project DLR 50WM 0346.

REFERENCES

- 1 B.P. Anderson, *Phys. Rev. A* **63**, 023404 (2001)
- 2 M.H. Anderson, J.R. Ensher, M.R. Matthews, C.E. Wieman, E.A. Cornell, *Science* **269**, 198 (1995)
- 3 K. Bongs, K. Sengstock, *Rep. Prog. Phys.* **67**, 907 (2004)
- 4 I. Bialynicki-Birula, Z. Bialynicka-Birula, *Phys. Rev. A* **65**, 063606 (2002)
- 5 S. Bize, P. Laurent, *C.R. Physique* **5**, 829 (2004)
- 6 C.C. Bradley, C.A. Sackett, J.J. Tollett, R.G. Hulet, *Phys. Rev. Lett.* **75**, 1687 (1995)
- 7 C.C. Bradley, C.A. Sackett, J.J. Tollett, R.G. Hulet, *Phys. Rev. Lett.* **79**, 1170 (1997)
- 8 K.B. Davis, M.-O. Mewes, M.R. Andrews, N.J. van Druten, D.S. Durfee, D.M. Kurn, W. Ketterle, *Phys. Rev. Lett.* **75**, 3969 (1995)
- 9 J.F. Dobson, *Phys. Rev. Lett.* **73**, 2244 (1994)
- 10 A. Fetter, J. Walecka, *Quantum Theory of Many-particle Systems* (McGraw-Hill, Boston, MA, 1971)
- 11 W. Greiner, *Mechanik*, Teil 2, 5th edn. (Verlag Harri Deutsch, Thun, 1989)
- 12 W. Hänsel, P. Hommelhoff, T.W. Hänsch, J. Reichel, *Nature* **413**, 498 (2001)
- 13 W. Ketterle, D.S. Durfee, D.M. Stamper-Kurn, in *Proc. International School of Physics – Enrico Fermi*, ed. by M. Inguscio, S. Stringari, C.E. Wieman (IOS Press, Amsterdam, 1999), pp. 67–176
- 14 W. Kohn, *Phys. Rev.* **123**, 1242 (1961)
- 15 S. Kraft, A. Deninger, C. Trüch, J. Fortágh, F. Lison, C. Zimmermann, *Laser Phys. Lett.* **2**, 71 (2005)
- 16 A.E. Leanhardt, *Science* **301**, 1513 (2003)
- 17 K.G. Libbrecht, J.L. Hall, *Rev. Sci. Instrum.* **64**, 2133 (1993)
- 18 G. Nandi, R. Walser, E. Kajari, W.P. Schleich, unpublished
- 19 H. Ott, J. Fortágh, G. Schlotterbeck, A. Grossmann, C. Zimmermann, *Phys. Rev. Lett.* **87**, 230401 (2001)
- 20 T. Petelski, M. Fattori, G. Lamporesi, J. Stuhler, G.M. Tino, *Eur. Phys. J. D* **22**, 279 (2003)
- 21 J. Reichel, W. Hänsel, T.W. Hänsch, *Phys. Rev. Lett.* **83**, 3398 (1999)
- 22 G. Schmid, *Phys. Rev. A* **15**, 1459 (1977)
- 23 J.H. Shirley, *Opt. Lett.* **7**, 537 (1982)
- 24 G. Wasik, W. Gawlik, J. Zachorowski, W. Zawadzki, *Appl. Phys. B* **75**, 613 (2002)
- 25 A.C. Wilson, J.C. Sharpe, C.R. McKenzie, P.J. Manson, D.M. Warrington, *Appl. Opt.* **37**, 4871 (1998)